Aquaculture 526 (2020) 735382

Contents lists available at ScienceDirect

Aquaculture

journal homepage: www.elsevier.com/locate/aquaculture

A pathomorphological description of cross-stitch vertebrae in farmed Atlantic salmon (*Salmo salar* L.)

Helle Holm[a,*], Elisabeth Ytteborg[b], Vibeke Høst[b], Anne Katrine Reed[a], Alf Seljenes Dalum[a], Grete Bæverfjord[c]

[a] Pharmaq Analytiq AS, Oslo, Norway
[b] Nofima AS, Postboks 210, NO-1431, Ås, Norway
[c] Nofima AS, Sjølsengvegen 22, NO-6600, Sunndalsøra, Norway

ARTICLE INFO

Keywords:
Atlantic salmon
Bone development
Cross-stitch
Deformity
Vertebrae
Axial lesions

ABSTRACT

[1]This study provides a pathomorphological description of a novel vertebral deformity in farmed Atlantic salmon, provisionally named "cross-stitch" vertebrae due to its characteristic pathological appearance by radiography. In worst cases, this vertebrae deformation is associated with reduced fish welfare, visibly deformed fish and increased risk of downgrading at slaughter due to connective tissue formation and discoloration of surrounding skeletal musculature. To describe and illustrate the pathological details of the affected vertebrae, radiographic techniques, histological methods and scanning electron microscopy were used. Vertebral dislocations, reduced intervertebral spacing and inwardly bent distal endplates (abaxial lesions) of vertebrae most frequently located caudally to the dorsal fin, characterized the radiographic appearance. Symmetrical radially distributed axial lesions in the proximal part of endplates were observed by computer tomography, scanning electron microscopy and by histological methods. These lesions have to our knowledge not previously been described in other vertebral malformations in Atlantic salmon. In detail, abnormal cartilage deposition between the endplates of adjacent vertebral bodies and in the intertrabecular adipose tissue, could suggest an attempt to stabilize the affected vertebrae. Abnormal bone growth was visualized with Picro Sirius staining, showing disorganized structures of the collagen fibers in the compact bone of the vertebral endplates and in the vertebral growth zones, features that were not observed in vertebrae without radiographic signs of "cross-stitch". Inter-trabecular inflammation containing a minor amount of myeloperoxidase (MPX^+) cells replaced the adipose tissue usually found in trabecular bone of healthy vertebrae, but inflammatory cells were in general not a predominant finding in the investigated stage of "cross-stitch" lesions. With the pathomorphological basis in place, additional studies are needed in order to define the conditions resulting in cross-stitched vertebrae.

1. Introduction

Farmed fish are affected by skeletal abnormalities. The occurrence is highly dependent on the species, rearing conditions and fish age (Boglione et al., 2013). In Atlantic salmon (*Salmo salar* L.), the most commonly cultured salmonid in the Northern Hemisphere, skeletal deformities are reported to occur in the skull and jaw (Berg et al., 2012; Bruno, 1990; Quigley, 1997; Sutterlin et al., 1987), opercula (Sutterlin et al., 1987) and spinal column (Aunsmo et al., 2008; Baeverfjord et al., 2009; Berg et al., 2012; Boglione et al., 2013). Although also present in wild Norwegian fish populations (Fjelldal et al., 2009b), deformities of the vertebrae have invariably been recognized as a substantial problem and welfare issue for farmed Atlantic salmon in Norway since the 1980s (Kvellestad et al., 2000; McKay and Gjerde, 1986; Vågsholm and Djupvik, 1998). Fish groups with high prevalence of vertebral deformities raise questions about animal welfare (Aunsmo et al., 2008; Fjelldal et al., 2009b; Huntingford et al., 2006; Kause et al., 2007), as the deformed spine may elicit pain and hinder normal activities such as the ability to swim and feed. In worst cases, spinal deformities severely affect the health and welfare of the fish and can also result in downgrading losses, such as growth impairment and reduced product quality (Kvellestad et al., 2000).

Depending on the site of development and number of affected vertebrae, abnormal body shapes such as body axis deviations and "short

* Corresponding author.
E-mail addresses: helle.j.holm.86@gmail.com (H. Holm), elisabeth.ytteborg@nofima.no (E. Ytteborg), vibeke.host@nofima.no (V. Høst), annekatrine.reed@zoetis.com (A.K. Reed), alf.dalum@zoetis.com (A.S. Dalum), grete.baverfjord@nofima.no (G. Bæverfjord).

https://doi.org/10.1016/j.aquaculture.2020.735382
Received 22 January 2020; Received in revised form 16 April 2020
Available online 19 April 2020
0044-8486/

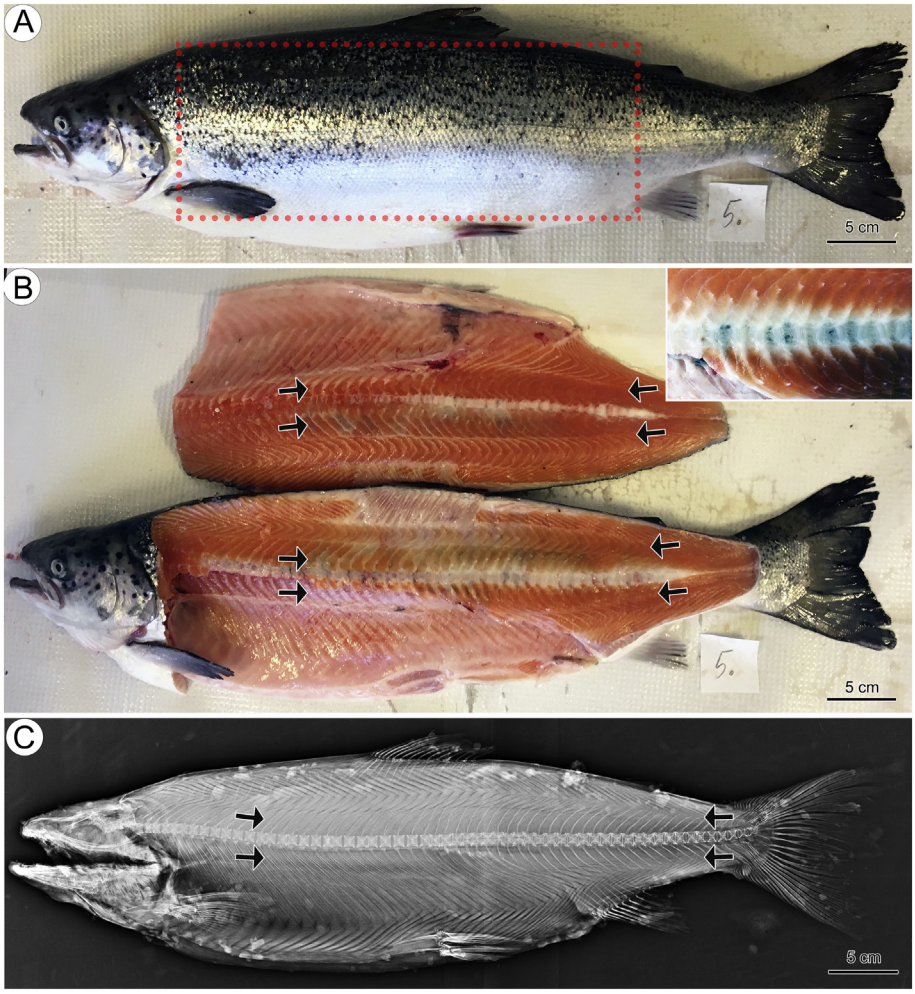

Fig. 1. Harvest-size Atlantic salmon with gross (A and B) and radiological (C) signs of cross-stitch pathology; all images from the same fish. A) Affected fish typically appear with a decreased body-length:-weight ratio and a slightly angular body-shape (accentuated by the red dotted rectangle). B) Necropsy; arrows point to pathological connective tissue formation and discoloration of the fillet in the perivertebral musculature surrounding cross-stitch lesions. Inset: details from pathological connective tissue formation and discoloration of perivertebral musculature. C) Arrows points to the corresponding region as shown in B, and the radiological image confirms cross-stitch pathology affecting in total 35 vertebrae. Note decreased intervertebral space between affected vertebrae and increased intervertebral space between seemingly normal vertebrae. Typically, affected vertebrae are found in groups of 2–3 vertebrae cranial to the dorsal fin, showing signs of vertical dislocation and reduced intervertebral space. Caudal to the dorsal fin, severely affected vertebrae are here found in one continuous piece, displaying severe pathoradiographic signs: inwardly bent distal endplates (abaxial lesions), irregularly craniocaudally compression of the vertebral body and the vertebrae appears fused to adjacent vertebrae. (For interpretation of the references to colour in this figure legend, the reader is referred to the web version of this article.)

tails", can be observed clinically (Boglione et al., 2013; Kvellestad et al., 2000; Silverstone and Hammell, 2002). The problem may be underreported since not all vertebral deformities are visible in the fish (Boglione et al., 2013; Åsgård et al., 1996). Minor deformities or developing deformities may only be found by advanced examination of the fish, e.g. by using X-ray, computer tomography (CT) or histopathological examination. Radiographic imaging is the most common method for diagnosing deformities and a categorization of vertebral malformations in Atlantic salmon into 20 groups was suggested (Witten et al., 2009). These comprise spinal curvature changes, like lordosis (V-shaped dorsal–ventral curvature), kyphosis (Y-shaped dorsal–ventral curvature), scoliosis (lateral curvature) and different pathological grades and combinations of platyspondyly (compressions) as well as fusions (Witten et al., 2009). Since pathomorphological changes in the bone structures may not be visible externally, vertebral malformations are often not diagnosed until later stages of the pathological development. It is therefore challenging to understand the cause of the deformity and its onset of development.

The Atlantic salmon vertebrae grows continually throughout life (Nordvik et al., 2005). The bone matrix (osteoid) of the endplates and trabeculae is mineralized through direct intramembranous ossification, while the arch centra is formed indirectly through endochondral ossification (Arratia et al., 2001; Bird and Mabee, 2003; Nordvik et al., 2005). These processes require a fine-tuned coordinated balance between the activities of the three main cells found in bone-tissue: the osteoblasts and the osteocytes entrapped inside the bone matrix, and the catabolic bone-resorbing osteoclasts. Together, these cells form and maintain the Atlantic salmon vertebrae and disturbances of their activity may lead to vertebral malformations exemplified by disturbed activity of osteoblasts and chondrocytes (Ytteborg et al., 2010a) and increased expression of stress related genes (Takle et al., 2005) after exposure to high temperature regimes early in life (Baeverfjord et al., 1998a; Takle et al., 2005; Ytteborg et al., 2010a). Mature osteoblasts mediate the osteoid production and mineralization of the osteoid matrix, of which the main minerals are calcium (Ca) and phosphorus (P) in Atlantic salmon vertebrae as in vertebrates in general. P-insufficiency may lead to structural changes, malformations and increased softness of the vertebrae (Baeverfjord et al., 1998b; Fjelldal et al., 2012; Helland et al., 2006; Sullivan et al., 2007; Witten et al., 2019). Controlled experimental studies have also linked family background (Gjerde et al., 2005), location (Sullivan et al., 2007), bacterial infections, chemicals (Madsen et al., 2001; Toften and Jobling, 1996), nutrition (Bou et al., 2017; Fjelldal et al., 2009a; Fjelldal et al., 2010; Madsen and Dalsgaard, 1999), vaccination (Berg et al., 2006), fish size at vaccination (Berg et al., 2006; Vågsholm and Djupvik, 1998) and combinations of these (Aunsmo et al., 2008; Grini et al., 2011) to the development of vertebral deformities.

This study addresses a seemingly novel type of skeletal deformity, which was first observed in commercially reared fish in Norway during the winter harvest season of 2016–17. The observations were made in fish submitted to the Nofima X-ray laboratory in Sunndalsøra, Norway for diagnostic purposes. The deformities were particularly severe, with comprehensive vertebral lesions and a substantial loss of growth towards harvest (Baeverfjord G., personal observations). The condition, for which etiology is unknown, was provisionally named "cross-stitch vertebrae" in order to provide a working name and distinguish from

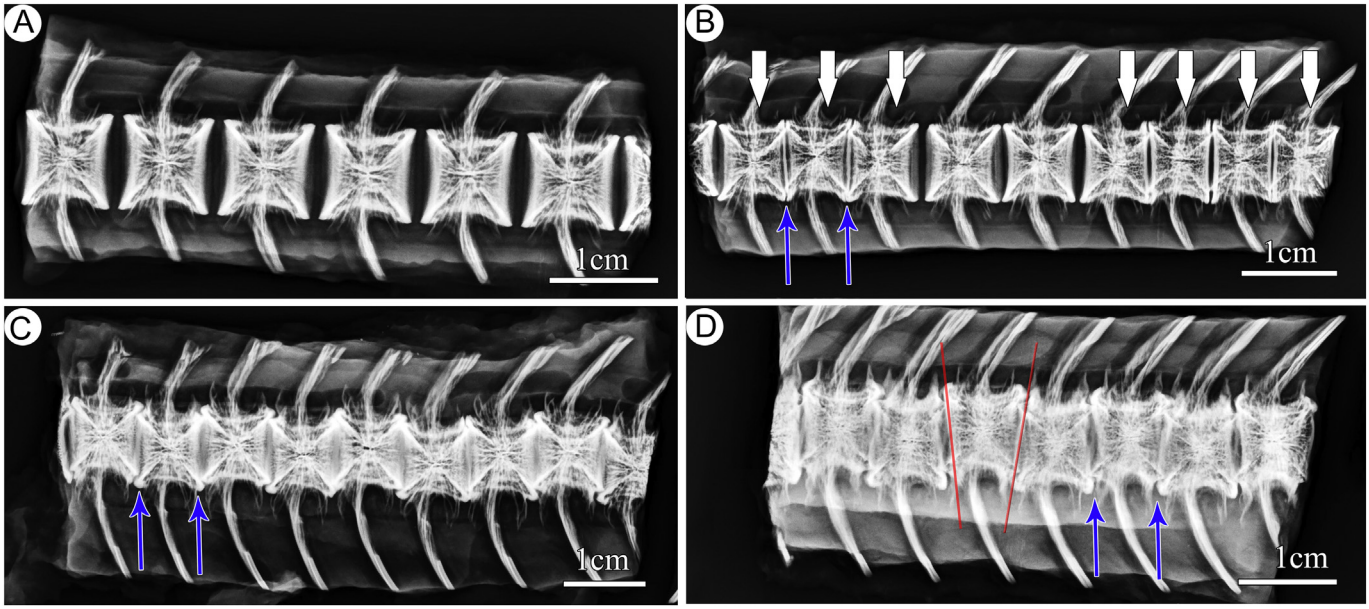

Fig. 2. Radiological images from Atlantic salmon showing A) normal vertebrae and B-D vertebrae with varying degree of cross-stitch pathology (all segments taken caudal to the dorsal fin). B) Early cross-stitch lesions in two different regions of the vertebrae (white block-arrows), causing narrowing of the intervertebral space between affected vertebrae and corresponding increased intervertebral space with adjoining normally shaped vertebrae. Blue arrows point to examples of abaxial lesions in the distal endplates (this also applies to the following images). C) Advanced lesions with loss of intervertebral space, extensive vertical displacement and inwardly bent distal endplates (abaxial lesions) affecting all vertebrae. D) Same as C but in addition irregularly craniocaudally compression of vertebrae into a wedge shape (accentuated with red lines for one vertebra) is observed. (For interpretation of the references to colour in this figure legend, the reader is referred to the web version of this article.)

other more common types of skeletal deformities. Through visual examination and by using different morphological techniques, including histopathological studies, scanning electron microscopy (SEM), computer tomography (CT) and X-ray, we describe pathomorphological details of the cross-stitch vertebrae. With these efforts, we hope to contribute with a fundament for further research into possible causal factors for the development of deformities of the cross-stitch type.

2. Material and methods

2.1. Animals

Harvest-size Atlantic salmon (3-5 kg) were sampled at three different slaughterhouses at coastal locations in Western and Central-Norway. The three fish populations were identified as risk groups by the producers, based on their production history and quality screening of similar fish groups.

At sampling, fish were selected from the production line in the slaughterhouse, following electrical stunning and bleeding. Selection of affected fish was performed based upon external appearance. Fish selected as suspected of having cross-stitch pathology ($N = 30$) were generally smaller than the group average and/or they displayed some degree of variation in body shape, having either a slightly angular shape (Fig. 1a) of the trunk of the body (visible particularly in the vent region) or a uniform shortness of the body trunk without any prominent bulges. Selected fish displayed one or more of these clinical signs. Following sampling of affected fish, a selection of fish normal on visual examination ($N = 28$) was performed. These were fish of average size for the group in total with normal body shape and a normal silvery skin tone.

Following selection, the fish were gutted and the left-side fillet was removed. Starting from just caudal to the dorsal fin, a 5–7 cm long section of the vertebral column was removed with surrounding muscle and connective tissue. This location was selected to standardize the sampling site because it appears to be a predilection site for cross-stitch vertebrae. From this piece, some of the soft tissue was carefully removed before the vertebral sample was immersed in 10% buffered (pH 6,8-7,2) formalin.

2.2. Radiography

2.2.1. X-ray Imaging

All the formalin-fixed pieces of the vertebral column were rinsed in saline water and X-rayed at the Nofima radiography laboratory in Sunndalsøra, Norway. The radiographic imaging was performed using a semi-digital computed radiography system (Fuji Medical AS, Oslo, Norway). Images were recorded on FCR Imaging Plates (Fujifilm, Tokyo, Japan) coated with photo-reactive phosphorus, and read by a FCR Profect Reader (Fujifilm, Tokyo, Japan). Image enhancement was performed automatically by the FCR console software, using fish size specific settings based on experience to obtain the best image quality. An IMS Giotto mammography X-ray (Giotto, Pontecchio Marconi, BO, Italy) source was used to achieve an image resolution of 20 pixels per mm^2, with exposure at 22 kV and 100 mAs, in combination with image plates with double-sided coating. Following radiography, the vertebral samples were stored in saline until processing for histology.

2.2.2. Computer Tomography (CT)

Ex vivo CT scans were carried out using a dedicated small-animal combined PET/CT scanner (Nanoscan PC, Mediso, Hungary) at the Department of Clinical Medicine at the University of Bergen (UIB). Formalin-fixed pieces of 5–8 vertebrae ($N = 6$ pieces of cross-stitched vertebrae, $N = 4$ pieces of vertebrae without radiographic signs of cross-stitch), after being rinsed in saline water were placed in a standard small-animal imaging bed and high-resolution CT images were acquired using an energy of 70 kVp, 300 ms exposure time and 720 projections. Images were reconstructed to a voxel size of $40 \times 40 \times 121$ M using a RamLak-filter. Images were analyzed using the InterView Fusion software (Version 3.01.021.0000, Mediso, Hungary).

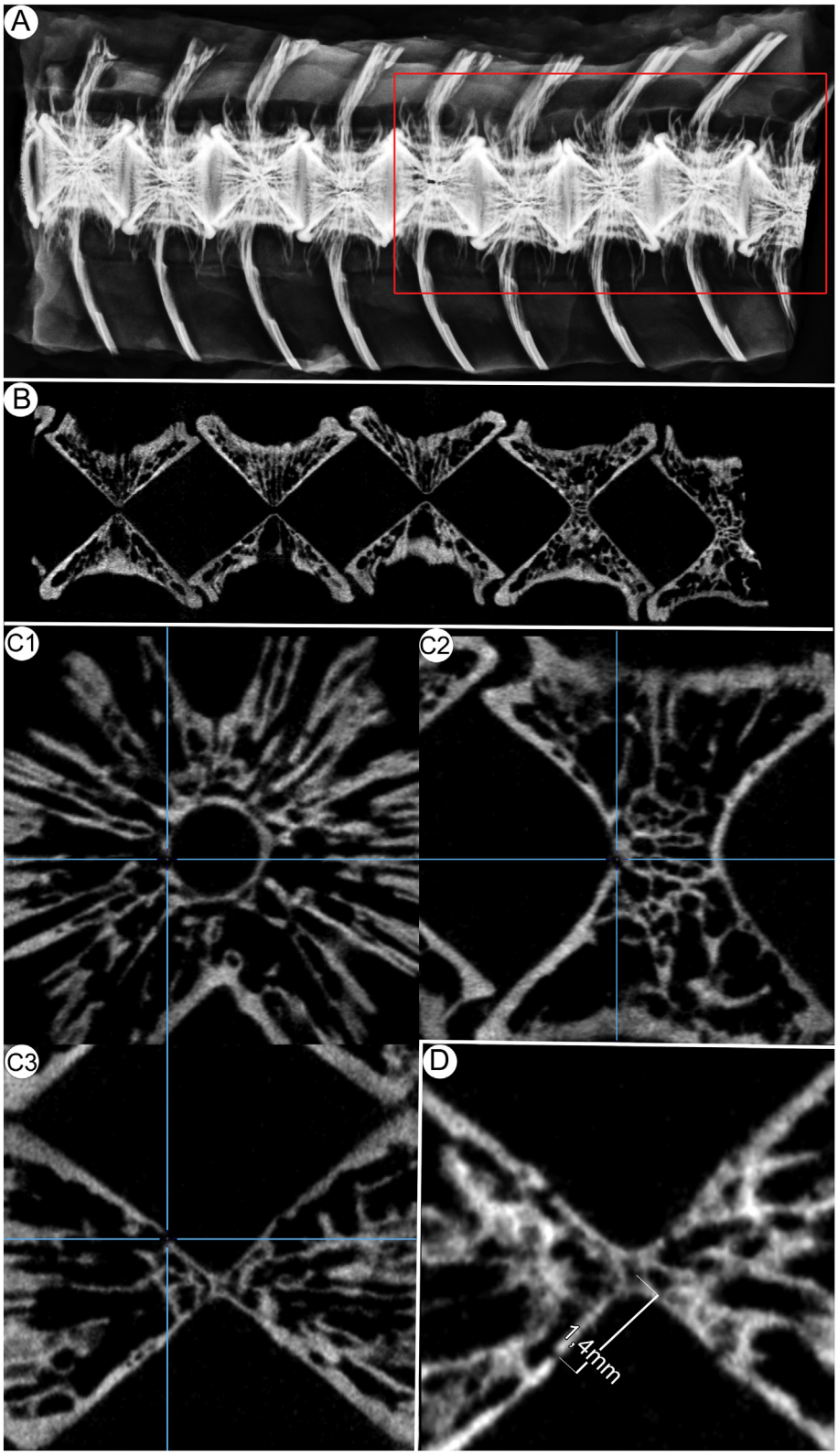

Fig. 3. Radiological images from Atlantic salmon with cross-stitch pathology. A represents X-ray, while B-D represents CT images of the same vertebral segment as seen in the red box in A. A) Extensive cross-stitch pathology affecting all vertebral segments and including narrowing of the intervertebral space, slightly vertical displacement of vertebrae and inwardly bent or displaced distal endplates (abaxial lesions). B) CT of medial plane or near medial plane of corresponding vertebrae as indicated with red box in A. Note shortening of intervertebral space, vertical displacement of vertebrae and displaced endplates. C) Transversal (C1), coronal (C2) and sagittal (C3) projection of the same vertebrae. Crossing of the blue lines indicates the same axial lesion of the proximal endplate seen in the different projections. D) Same vertebra and projection as C3 but aligned for optimal viewing of the axial lesions. Approximate measurement of distance from the approximate middle of the vertebra to one axial lesion is indicated in the figure. (For interpretation of the references to colour in this figure legend, the reader is referred to the web version of this article.)

2.3. Scanning Electron Microscopy (SEM)

Formalin-fixed pieces of 5–8 vertebrae from individuals (N = 8) with radiographic signs of cross-stitch pathology and vertebrae from individuals (N = 8) showing no radiographic signs of pathological development in their spines, kept in saline water, were analyzed by SEM. Soft tissue was removed by submerging the vertebral segments into 10% potassium hydroxide (KOH) overnight at 37 °C, followed by rinsing in tap water. This procedure was repeated until all soft tissue was removed. Decalcination was necessary in order to enable dissection of the vertebrae in the medial plane, and this was done by submerging the vertebral segments without soft tissue in 4.0 M formic acid containing 3.4% *w/v* sodium formate for 24 h at room temperature. For evaluation of the vertebrae and their endplates in cranio-caudal

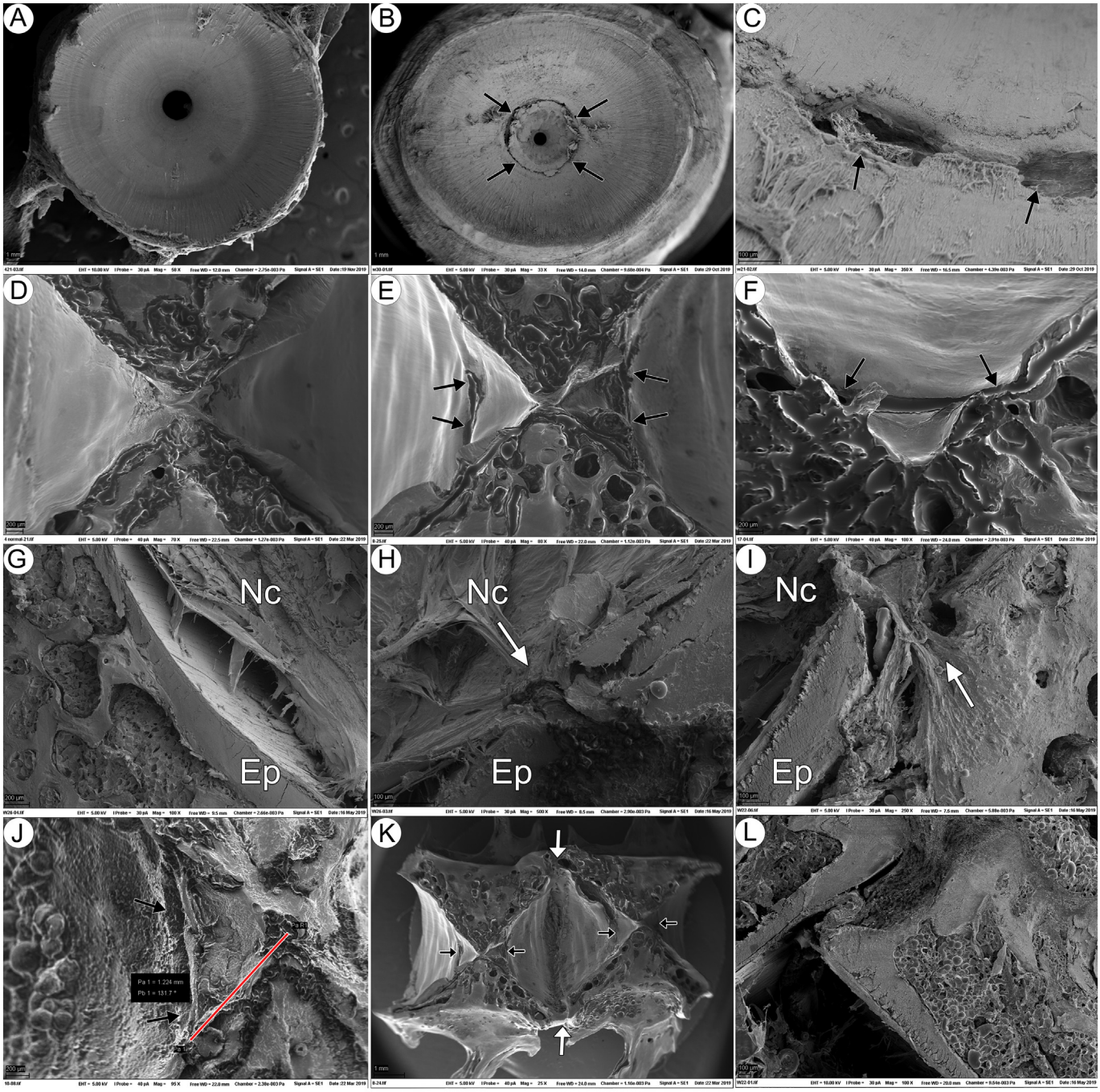

Fig. 4. Scanning electron microscopy from Atlantic salmon vertebrae with normal appearance (A, D and G) or with cross-stitch pathology (rest). The vertebrae are either viewed in craniocaudal projection (A-C) or mediolateral projection of vertebrae cut in near-medial plane (D-L). In A-F and J-L, the notochord was removed during tissue processing. A) Normal vertebra showing a smooth surface of the entire endplate of the vertebrae facing the intervertebral space. B) Circular distribution of axial lesion close to the center channel of the vertebra (black arrows). C) Details from the axial lesion seen in B, showing a minute disruption of the compact bone of the endplate (black arrows). D) Normal vertebra. E) Axial lesion (black arrows). F) Details of axial lesion (black arrows). G) Cut surface of normal vertebra with a continuous endplate separating notochord (Nc) residing in the intervertebral space from surrounding spongy trabecular bone tissue. H) Minute disruption of the proximal endplate and probable leakage of notochord through the end plate disruption into caverns of trabecular bone (white arrow). I) Minute disruption of the proximal endplate and likely leakage of inter-trabecular soft tissue through the disruption into the intervertebral space (white arrow). J) Approximate measurement of the length from the center channels to the axial lesion (length of red bar): 1.22 mm. K) Overview of two vertebrae with vertical displacement and abaxial lesions at the distal endplates (white arrows). Black arrows point to axial deformities. L) Details from abaxial lesions showing the distal part of two dislocated endplates folding upon each other. (For interpretation of the references to colour in this figure legend, the reader is referred to the web version of this article.)

projection, no decalcification was needed. All specimens were further dehydrated in 100% ethanol (EtOH) and dried using a Critical Point Dryer (CPD 030, Bal-tec AG, Schalksmühle, Germany) with liquid carbon dioxide as the transitional fluid. The samples were then mounted on stubs with carbon tape and coated with gold-palladium (Polaron Emitech SC7640 Sputter Coater, Quorum technologies, East Sussex, United Kingdom) and examined by SEM (EVO® 50 Series, Carl Zeiss AG, Oberkochen, Germany).

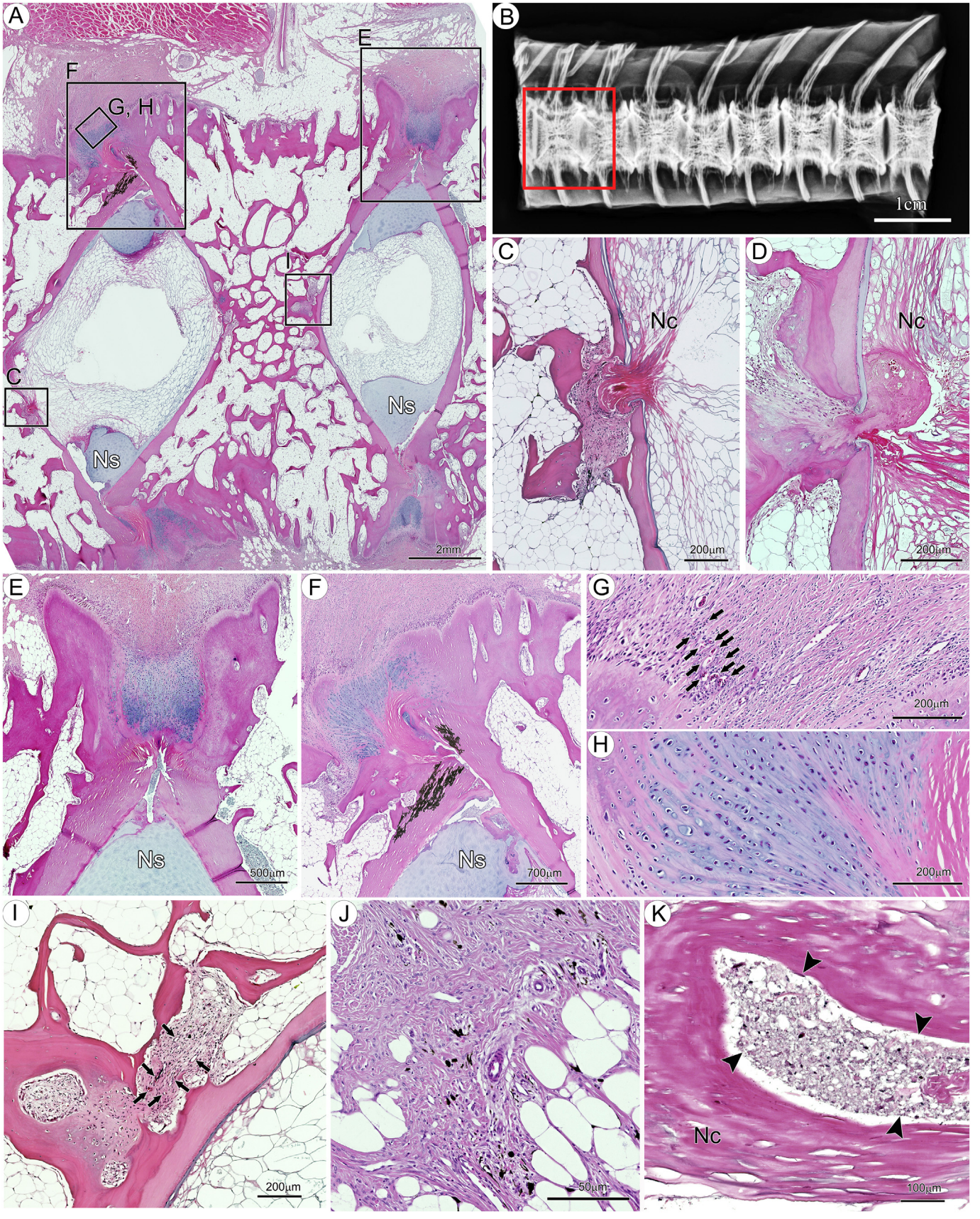

(caption on next page)

Fig. 5. *HE*-staining and X-ray of cross-stitch pathology in Atlantic salmon vertebrae. A) Overview of one whole vertebra and the halves of two adjoining vertebrae, all showing signs of cross-stitch pathology. Boxes with letters indicates regions of magnification in following images (black region in the image (seen in higher magnification in F) represents an artefact due to entrapment of air between tissue, mounting media and cover slip causing distortion of the light path). B) X-ray image acquired of the same vertebrae before histological processing. Red box indicates corresponding region as shown in A. C) Axial lesion with minute disruption of the compact bone of the endplate and probable displacement of notochordal tissue (Nc) through the disruption into inter-trabecular soft tissue. D) Axial lesion with minute disruption of the endplate and probable displacement of inter-trabecular soft tissue through the disruption into the intervertebral space. E) Abaxial lesion where the osteogenic zones of the distal endplates of two adjoining vertebrae display deviation. F) Abaxial lesions with folding of one distal endplate over the adjoining distal endplate with extensive tissue disruption in the osteogenic zone. G) High magnification of disruption of osteogenic zone. Arrows points to vascular structures. H) Cartilage cells of the osteogenic zone appear disorganized. I) Abnormal tissue replacing the inter-trabecular adipose tissue normally contained in the spaces within the trabecular bone. The tissue consisted of a mix of cartilaginous tissue, connective tissue, signs of neovascularization and inflammatory cells and were commonly found adjacent to the axial lesions. J) Cells containing black pigments, presumably melanocytes or melanomacrophages, were a common finding in association with cross-stitch pathology, here seen in excessive connective tissue formations surrounding the endplate. K) Cell-remnants and debris that resemble degenerated erythrocytes within spaces which likely represent the extracellular lacunae in the notochord. Ns; notochord sheet. (For interpretation of the references to colour in this figure legend, the reader is referred to the web version of this article.)

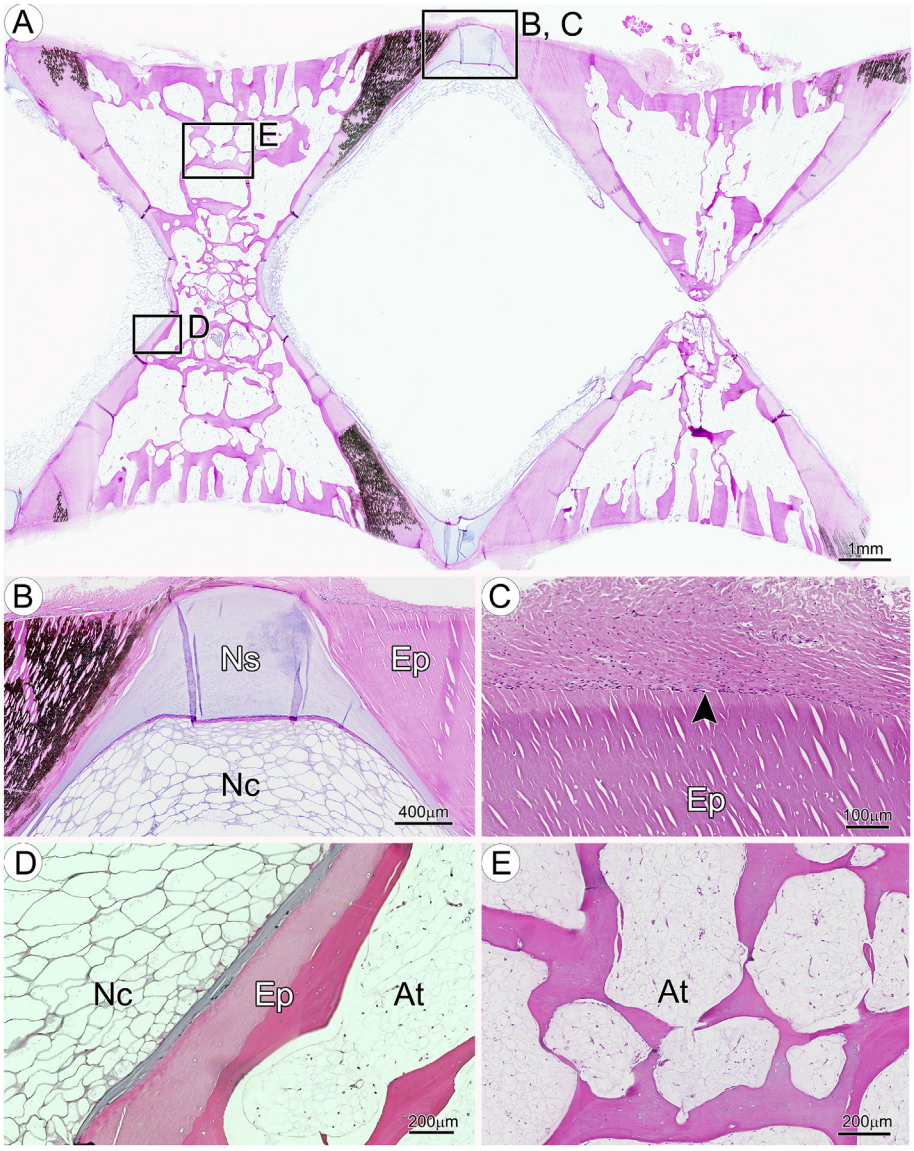

Supplementary Fig. 8. HE-staining of apparently normal Atlantic salmon vertebrae. A) Overview of two whole vertebrae in near-medial orientation. Boxes with letters indicate regions of magnification in following images (black region in the image (seen in higher magnification in B) represents an artefact due to entrapment of air between tissue, mounting media and cover slip causing distortion of the light path). B) Distal endplate (Ep) with growth zone, notochord sheet (Ns) and notochord (Nc). C) Transition between distal endplate and growth zone (arrowhead). D) Proximal part of endplate surrounded by notochord and inter-trabecular adipose tissue (At). D) Trabecular bone and inter-trabecular adipose tissue.

2.4. Histology and immunohistochemistry

The formalin-fixed pieces were reduced in size to 2–4 consecutive vertebrae in order to be properly processed and to fit the embedding cassettes. These pieces belonged to individuals (N = 20) with radiographic signs of cross-stitch pathology and vertebrae from individuals (N = 4) showing no radiographic signs of pathological development in their spines. Decalcination was performed in 10% EDTA at pH 7 and at room temperature for 2–3 days before processing in an automated tissue processor (TP1020, Leica Biosystems, Germany) where the samples were dehydrated with 100% ethanol followed by a clearent xylene bath and infiltration in melted paraffin (Histowax, HistoLab, Sweden) at 60 °C. Paraffin-embedded tissue samples were sectioned parasagittaly close to the center of the vertebrae (midsagittal level), at 5 µm thickness using a Leica RM 2165 Microtome (Leica Biosystems, Germany) mounted on glass or polysine coated slides (VWR, Norway)

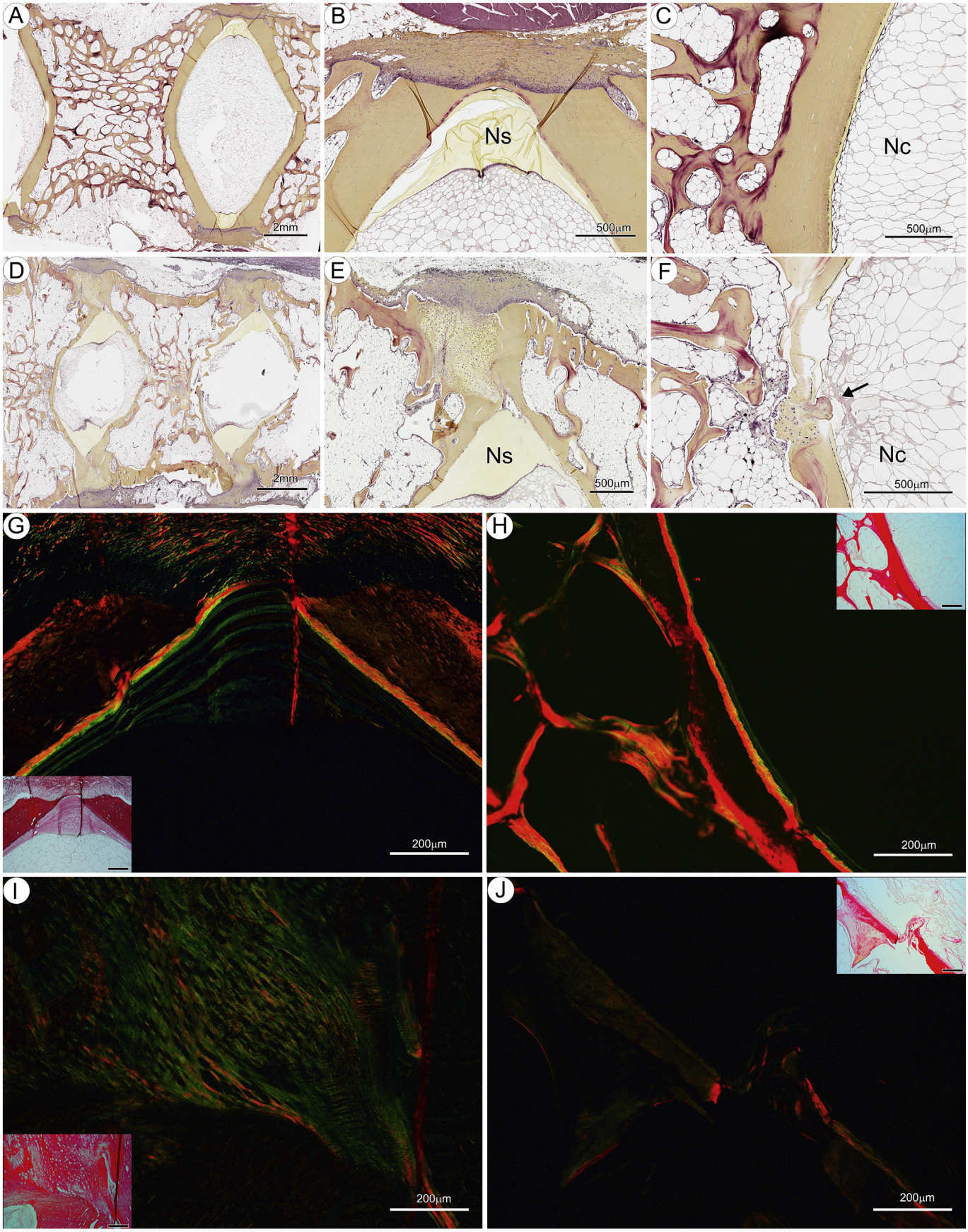

(caption on next page)

Fig. 6. Movat (A-F) and Picro Sirius (G-J) staining of harvest-size Atlantic salmon vertebrae showing normal vertebrae in A-C, G and H, images D-F and I and J show vertebrae with cross-stitch pathology. A) Overview of one whole vertebral body and one half of one adjoining vertebra showing the intervertebral space and the notochord. Enlarged images of B) showing the vertebral growth zones of two adjacent vertebrae and C) the compact bone of the endplate and the trabeculae. D) Similar overview of vertebra with cross-stitch pathology. Enlarged images of E) the vertebral growth zones with ectopic cartilage between the vertebral distal endplates (abaxial lesion) and F) ectopic cartilage in the breach in the proximal endplate (axial lesion). Picro Sirius stained vertebrae show differences in the collagen distribution. Vertebrae showing normal phenotype had larger collagen fibers (type 1, stained red) in both the G) vertebral growth zones and in the H) trabeculae, compared to vertebrae with cross-stitch pathology showing smaller collagen fibers (e.g. collagen type 4, green) with more disorganized structure in both the growth zones (I) and in the trabeculae (J). Ns; notochord sheet, Nc; notochord. (For interpretation of the references to colour in this figure legend, the reader is referred to the web version of this article.)

and dried overnight at 37 °C. The sections were deparaffinized, rehydrated and stained with hematoxylin and eosin (HE) according to standard procedures. In addition, the Russel-Movat Pentachrome Stain (Rentsch et al., 2014) and Picro Sirius stain (Catalog No. 24901, Picro Sirius Red Stain Kit, Polyscience, Inc. US) were used according to the manufacturer's protocol on a subset of the samples.

Several different commercially available antibodies were used to study the cells involved in the deformed vertebrae in more detail by using immunohistochemical (IHC) techniques. For identification of myeloperoxidase positive (mpx^+) cells as a proxy for the involvement of inflammatory cells, we used the commercially available polyclonal anti-zebrafish myeloperoxidase from GeneTex (GTX128379, Irvine, California, United States). Myeloperoxidase is an abundant heme-containing enzyme present in neutrophils, monocytes, and macrophages (see (Klebanoff et al., 2013; Shaeib et al., 2016) and references therein). For detection of components in the extracellular matrix, collagen 1a1 (ab 23,730, AbCam, UK) was used. To detect cells undergoing apoptosis, active caspase 3 (Cleaved-G7481, Promega, USA) was used. See supplementary file 1 for description of methods.

The slides were examined by light microscope (Leica Microsystems), while Picro Sirius stained sections were examined in polarized light. The Leica Application Suite X (LAS X) software platform was used to photograph the sections.

3. Results

3.1. Clinical signs and gross pathology

Macroscopic signs in fish sampled as “affected” for the study corresponded to those previously observed in fish diagnosed with cross-stitch vertebrae by X-ray. In general, affected fish were smaller than the group average. Body shape deviations were categorized into two main types; a slightly angular shape, which compared well to previous observations in moderately affected fish (Fig. 1A), or a more prominently shortened, rounded shape in some fish, which compared to severely affected fish in which the whole vertebral column was affected. Vertebral pathology was observed after filleting. Parts of the vertebral columns were compressed and rigid, with a perivertebral sheath of thick and tough connective tissue surrounding the compressed vertebral regions. A variable degree of muscular pathology was observed in affected fish: pale and discolored muscle, sometimes with dark-pigmented shadows deep in the muscle (Fig. 1B). On closer inspection, the transition between the vertebral column and surrounding soft tissue was abnormally rigid with strands of white connective tissue growth protruding from the spine and into the perivertebral musculature. In some individuals, dark melanin-like spots were seen inside the vertebral bone (Fig. 1B, inset). The pathological lesions appeared to be most pronounced in vertebrae caudal to the dorsal fin. In fish with normal external features, none of these autopsy findings were observed.

3.2. Radiographic Imaging

Material available for radiography was formalin-fixed pieces of vertebral column, which comprised 5–8 individual vertebral bodies sampled from just caudal to the dorsal fin. Of the 30 fish classified as ‘affected’ by gross morphology, cross-stitch lesions were observed in 28 fish. Two fish had no lesions in the radiographed vertebral piece and appeared radiologically normal. Correspondingly, 7 of the 28 fish classified as ‘normal’ had unequivocal signs of the same pathology.

The radiographic details for diagnosing cross-stitch by radiographic imaging were interpreted as a condition with a progressive pathological development. In mild cases, vertebral radiographic changes (lateral view) were vertical displacement and reduced intervertebral space of one or more segments including 2–3 adjacent vertebrae, interspersed by groups of seemingly normal structures (Fig. 2B). The individual vertebrae were normally shaped with the X-shape easily observed. In more advanced cases, the lesions comprised higher numbers of affected vertebrae (Fig. 2C). The squared X-shape of each vertebra was mostly retained, but the distal ends of endplates appeared inwardly bent, either pressed and/or folded over each other (abaxial lesions, Fig. 2B-D). Intervertebral spaces were absent, and vertical displacement between adjacent vertebrae appeared throughout (Fig. 2C). This stage gave rise to the term “cross-stitch vertebrae”, due to its superficial likeness to cross-stitch embroidery. In what appeared to be further progressed lesions, the vertebrae were irregularly craniocaudally compressed into a wedge shape and dislocated dorsally and ventrally (Fig. 2D). Severely affected fish had deformed vertebrae lacking intervertebral spacing to adjacent vertebrae in one continuous piece (Fig. 1C), resulting in > 50% of the spine being affected in some cases. Adjacent intervertebral spaces between radiographically normal vertebrae were often elongated, likely due to attempts to compensate for the areas of vertebral shortening (Fig. 2B). Interruptions in the proximal part of the endplate, the axial lesions, were observed by CT in all three projections (transversal, coronal and sagittal view, Fig. 3C), with an approximate distance of 1.4 mm from the vertebra central channel (Fig. 3D).

3.3. Scanning Electron Microscopy (SEM)

In vertebrae affected by cross-stitch pathology, a ring-shaped structure in the proximal endplates were observed by cranio-caudal SEM projection (Fig. 4B). The ring structure appeared as perforations of the proximal endplate (Fig. 4C). Higher magnification of near-medially cut vertebrae revealed that these perforations were indeed a breach/fracture in the compact bone of the proximal endplate (Fig. 4E, F, H, I and J). Approximate measurement of the length from the centre channels to the axial deformity showed that the ring structure was located about 1.2–1.6 mm from the vertebral center in all samples analyzed (Fig. 4J). Notochordal tissue seemed to leak out of the breach in some affected vertebral bodies (Fig. 4H), while inter-trabecular soft tissue moved out into the notochordal tissue in other samples (Fig. 4I). SEM further revealed changes in the growth zones in the distal endplate (abaxial lesions), with ectopic tissue formation in the intervertebral space (Fig. 4K and L). Similar pathological findings were not found in samples of vertebrae without radiographic signs of cross-stich pathology (Fig. 4A, D and G).

3.4. Histopathological Description of Cross-stitch Lesions

3.4.1. Hematoxylin and Eosin Stain

Consistent findings in all vertebrae presented with cross-stitch lesions (verified by radiography) could be divided into three pathological entities: I) Axial deformations and lesions of the compact bone of the

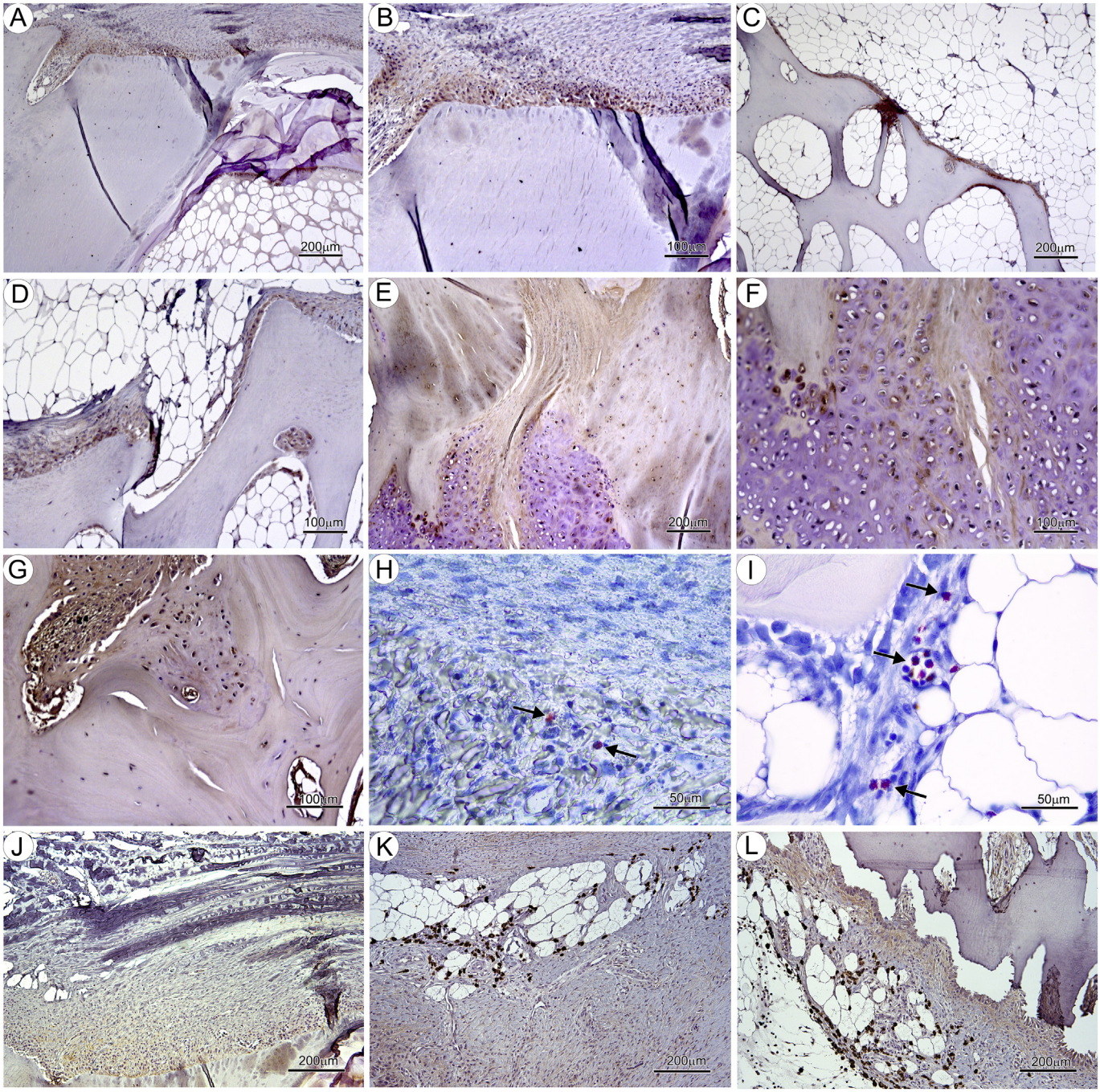

Fig. 7. Immunohistochemistry of Atlantic salmon vertebrae with normal appearance (A-D and J) or with cross-stitch pathology (E-I, K and L). All vertebrae cut in the medial or sagittal plane. A-G and J-K were stained against collagen 1a (Col1a) and caspase 3 respectively where brown staining (DAB) indicates positive reaction, while H and I were stained against myeloid-specific peroxidase (MPX) where red staining (AEC) indicates positive reaction. A) Normal appearance of Col1a$^+$ osteoblasts in the growth zone of the vertebrae. B) Same as A at higher magnification. C) Normal appearance of Col1a$^+$ osteoblasts lining the intravertebral spongy trabeculae tissue. D) Same as C, at higher magnification. E) Positive reaction for Col1a in ectopic cartilage in the growth zone of the vertebra. F) Same as E, at higher magnification. G) Positive staining of Col1a in inter-trabecular soft tissue. H) Slight numbers of MPX$^+$ cells in the growth zone of a cross-stitch vertebra. I) Slight numbers of MPX$^+$ cells in the inter-trabecular soft tissue of a cross-stitch vertebra J) Caspase 3-staining of the distal endplate from a vertebra with normal appearance. K) Caspase 3$^+$ cells in area of abaxial cross-stitch pathology of perivertebral soft tissue. L) Caspase 3$^+$ cells in perivertebral soft tissue away from the endplate. (For interpretation of the references to colour in this figure legend, the reader is referred to the web version of this article.)

endplate, II) Replacement of adipose tissue in the trabeculae with fibrous tissue and immune-like cells, III) Abaxial pathological changes. The morphology of each entity is illustrated with HE stained sections in Fig. 5.

Axial deformations (axial lesions) of the compact bone of the endplate, affecting both the cranial- and caudal facing endplate within the same vertebra (Fig. 5A, C and D) were found in vertebrae with radiographic signs of cross-stitch pathology. These lesions were located close to the center of the vertebra, and from observations, appeared about 1.2–1.6 mm from the vertebral center, meaning that these lesions only could be visualized in sections from medial to near-medial regions of the vertebrae. However, the distances from the center of the vertebrae to axial deformities were not subjected to systematic, statistical analysis in this material. Depending on the section depth, seemingly

different tissues could be observed associated with the lesions of the compact bone. Parallel sections of these observations revealed discontinuities and clear breaks of the endplates with prolapse of the notochordal tissue into inter-trabecular soft tissue (Fig. 5C) or fibrous tissues from the inter-trabecular soft tissue protruding into the intervertebral space (Fig. 5D). The abaxial changes were extensive (Fig. 5E and F). The distal endplates were pressed towards one another resulting in significantly reduced intervertebral space. In some cases, the endplates appeared symmetrically pressed towards one another (Fig. 5E). In other cases, the endplates were shifted vertically so they appeared rotated (Fig. 5F). This resulted in a seemingly thickened intervertebral ligament being displaced and pulled into the dislocated lesion. The intervertebral area contained metaplastic cartilaginous and chondroid tissue fusing the distal endplates together (Fig. 5E-H). The bone producing cells, the osteoblasts, at the vertebral growth zone appeared disorganized, with a seemingly increased number of blood vessels (Fig. 5G). Between the trabecular bone in the spongiosa, both near and away from the axial deformities, adipose tissue was frequently replaced with cartilaginous tissue, fibrous tissue and immune-like cells (Fig. 5I). Melano-macrophages were infrequently observed in these areas (Fig. 5J). The inflammatory material was often observed to be continuous over larger areas, suggesting a lytic effect on the bone tissue. In the space between the osteogenic zones and the notochord sheet or in empty spaces within the notochord that could represent remnants of the extracellular lacunae within the notochord, areas with partially or fully degraded red blood cells were often observed (Fig. 5K).

These histopathological changes could not be found in the control fish (supplementary Fig. 8) that had vertebrae without pathological findings as assessed from radiographical examination.

3.4.2. Special stains

To further elaborate on the pathological observations made by HE stains, sections were stained with Movat (Fig. 6D-F), which is intended for use in histological staining of collagen, elastin, muscle, mucin and fibrin in tissue sections (Rentsch et al., 2014). In vertebrae with cross-stitch pathology, ectopic cartilage formation was visualized between the distal endplates of adjacent vertebral bodies (abaxial lesions, Fig. 6E), by the axial lesions of the endplate and in the adipose regions of the trabeculae (Fig. 6F). Cartilage deposition in the intervertebral regions (Fig. 6E) resulted in bridging of the two vertebral endplates as observed with HE-staining. Picro Sirius was further used to stain collagenous tissue and revealed differences in collagen types in the affected areas (Fig. 6G-J). In the intervertebral regions, collagen 1 was absent, as expected. Collagen 1 was found in the compact bone of the endplate in both vertebrae without malformations and in the cross-stitch vertebrae. Staining with Picro Sirius visualized disorganized structures of the collagen fibers in the compact bone of the endplates in both axial- and abaxial lesions of vertebrae with cross-stitch pathology (Fig. 6I and J).

3.4.3. Immunohistochemistry

Collagen 1a antibodies showed positive staining in the osteoblasts at the vertebral growth zones and along the rims of the trabeculae in normally shaped vertebrae (Fig. 7A-D). Only the bone lining osteoblasts (both in the compact bone and in the trabeculae) and osteocytes stained positive in vertebrae without radiographic signs of cross-stitch pathology. Mixed signals from cells in the intervertebral ectopic cartilage were found in cross-stitch vertebrae, where cells dislocated from the growth zones were collagen 1a negative and those still attached to the growth zones were collagen $1a^+$. This indicates a combination of different cell types in these regions (Fig. 7E, F). In the trabeculae, collagen $1a^+$ cells were found in the inter-trabecular soft tissue replacing the adipose tissue (Fig. 7G). In vertebrae with cross-stitch pathology, the MPX antibody showed reactivity to individual cells in the growth zones and in the areas of inter-trabecular inflammation described in paragraph 3.4.1. Positive cells were solitary and found in clusters. MPX^+ cells were not found in the adipose tissue contained in the trabecular bone in vertebrae without radiographic signs of cross-stitch. Caspase 3 visualize cells undergoing apoptosis (programmed cell death). There were few caspase 3^+ cells in vertebrae without signs of cross-stitch, however they were numerous in affected vertebrae (Fig. 7J-L). Most of the positive cells were found in the surrounding connective tissue.

4. Discussion

This study gives a detailed pathological description revealing that the cross-stitch vertebrae in Atlantic salmon is a specific vertebral deformity with some unique pathological features. The gross pathology and radiographical observations in the present material was similar to what is observed in previously diagnosed Atlantic salmon. Consistent pathological findings in all vertebrae with cross-stitch lesions and examined with the different methods used in this study. These could be divided into the following: I) Axial radially distributed lesions in the compact proximal endplate, II) Replacement of adipose tissue in the trabeculae with fibrous tissue and immune-like cells, III) Abaxial lesions in distal endplates, IV) dislocation of vertebral bodies with reduced to absent intervertebral space with secondary changes; cartilage metaplasia and in advanced cases; irregular craniocaudal compression of the vertebral bodies. Depending on the degree of vertebral deformities, various amounts of perivertebral fibrosis and discoloration of adjacent musculature was seen clinically. We suggest that the axial deformation of the endplate is the primary cause for cross-stitch pathology, as discussed below.

4.1. Primary pathological changes

The radially distributed axial lesions of the end plates as found by SEM (confirmed by CT and histology) has to our knowledge never been previously described in studies of vertebral malformations in Atlantic salmon. This lesion is easily overlooked without thorough examination. From histological, SEM and CT investigations, the axial lesions in the compact bone of the affected endplate could be detected at an equal distance (1.2–1.6 mm from the vertebral center, approximate distances) from the central canal. The location of the lesions mean that they were only visible in medial or close-to-medial histological sections, thus inferring a circular distribution of anomalies to the compact bone. Radial distribution of the lesion was confirmed by SEM-investigations. Situated at the cranial and caudal edges of the endplates, the osteoblasts produce collagen rich osteoid that later mineralizes. It has been suggested that defects predominating at the distal location of the vertebral endplate is often owed to specific etiologies (Lotz et al., 2013). With this in mind, it is tempting to speculate about local disturbances in the osteoblast rich growth zone at an early age of the affected fish, with temporary damage to the growth zone at an early age coinciding with the axial deformity as seen in older individuals. Thus, if this lesion occurred early in life, it most likely occurred during the smolt stage in freshwater, or latest during the early post-smolt period. If this is the case, a disturbance in the osteoblast activity at the growth zones could have caused a weakness in the compact bony structure of the endplate, that later fractures from increased pressure caused by growth of the vertebrae and possibly increased stress from the surrounding skeletal musculature as the fish grows. This would explain the cartilaginous tissue found in these regions, as cartilage is often used as a compensatory tissue in deformed vertebrae in salmon (Witten et al., 2005; Ytteborg et al., 2010a). In a recent paper by Trangerud et al. (2020) describing similar vertebral deformities in Atlantic salmon, a significant association between gas within the notochord and vertebral lesions was shown. However, the possible association between observed gas and vertebral deformities was not further discussed in the paper, and gas-bubble formation was not observed in our material. When compared to the pathological details described for other categories of vertebral deformities in fish, the axial, radially distributed lesions of the compact

bone appear to be unique for cross-stitch deformed vertebrae.

4.2. Secondary pathological changes

The affected vertebrae were most often located in the highly mobile caudal section of the spine. As the fish grows and acquires an increased muscular mass and increased length of endplates, a substantial force would be expected to act on the initial axial defect of the endplate. Movement in the compact bone of the vertebrae distal to the suggested initial endplate anomaly could easily cause tissue disturbances both in the distal growth zone of the vertebrae as well as soft tissue alterations as seen in cross-stitch lesions. Reduced or absent intervertebral space was a common finding. Using histology, it was observed that the endplates of opposing vertebrae appeared staggered to each other, most likely a result of displacement of the vertebrae in relation to each other. In the space between such opposing endplates, varying degree of cartilage-metaplasia was noted, explaining why cross-stitch vertebrae often appeared fused by radiographic imaging. The cartilaginous tissue probably stems from the interrupted growth zone of the axial-most growth-zone, as also described in fused vertebrae (Witten et al., 2005; Ytteborg et al., 2010b). Another similarity with the pathological findings found in vertebral fusions of Atlantic salmon is the disorganization of collagen $1a^+$ cells, which likely represents osteoblasts. These cells could be in a state of transition from intramembranous ossification to endochondral bone formation through a stage of ectopic cartilage production (Witten et al., 2005; Ytteborg et al., 2010b). Picro Sirius staining of the endplates revealed a disorganized structure of the collagen fibers, suggesting that the organized pattern of matrix deposition from the osteoblasts was disturbed at an earlier timepoint than at slaughter of the fish.

Overload caused by mechanical forces, such as from the strong muscle mass in farmed Atlantic salmon, could hypothetically result in the radiologically observed vertical dislocation/displacement of adjacent vertebrae and collapse of the intervertebral space that reduce the spinal flexibility. The following direct bone-to-bone contact may further stimulate heterotopic cartilage deposition in the intervertebral area. This pathological phenomenon, that resembles a pseudoarthrosis (a false joint), can occur in humans due to failed attempted spinal fusions (see (Leven and Cho, 2016) and references therein). Furthermore, the trabecular areas containing fibrous inflammatory material, including MPX^+ cells, suggest a state of chronic active inflammation which could represent an ongoing attempt to heal or stabilize the initial lesions. In most terrestrial animals, deformities and fractures in compact bones are usually healed efficiently, and central to the direct (primary) healing process in the presence of Haversian channels (Weisbrode, 2007). Teleost fish lack such arrangement, and it has therefore been argued that fish have less efficient ways of repairing bone deformities (Roberts and Rodger, 2012). Atlantic salmon do however have active osteocytes believed to take an active part in bone maintenance and strengthening during growth (Ytteborg et al., 2013). It is interesting that osteocytes in non-deformed vertebrae were collagen $1a^+$, whereas few osteocytes in cross-stitch vertebrae showed positive staining. The role of these cells in the pathological development of cross-stich deformed vertebrae is not known, but it is probable that the quality of older bone in these animals has deteriorated. However, this consideration is based upon speculations and controlled experimental trials are needed to investigate the pathological mechanisms leading up to the cross-stitch vertebrae deformity complex. In such trials we believe that inclusion of early life-stages will be important.

5. Conclusion

In this report, we describe pathological details characteristic for this novel vertebral deformation, forming the fundament for further research and monitoring of this emerging condition. The mechanism behind the development of cross-stitch vertebral deformities is currently unknown, and controlled experiments elucidating various risk factors are needed in order to get clear insight into disease development and prevention.

Supplementary data to this article can be found online at https://doi.org/10.1016/j.aquaculture.2020.735382.

Acknowledgements

This study was supported by The Norwegian Seafood Research Fund (FHF), project number 901430. We would like to thank the industrial partners in this project for their support and the slaughterhouse staff for assistance with sampling of fish. The authors are also grateful to Randi Grøntvedt (INAQ) for identification of relevant fish groups and Kjellrun Gannestad (Nofima) for excellent technical assistance throughout the project. SEM imaging was performed at the Imaging Centre, Faculty of Biosciences, Norwegian University of Life Sciences with superb support from Lene Hermansen and Hilde Kolstad. CT scans were performed at the Department of Clinical Medicine at the University of Bergen (UIB) with brilliant help from Heidi Espedal.

Declaration of Competing Interest

The authors declare that they have no known competing financial interests or personal relationships that could have appeared to influence the work reported in this paper.

References

Arratia, G., Schultze, H.P., Casciotta, J., 2001. Vertebral column and associated elements in dipnoans and comparison with other fishes: development and homology. J. Morphol. 250, 101–172. https://doi.org/10.1002/jmor.106210.1002/jmor.1062.

Åsgård, T., Holmefjord, I., Gjerde, B., Baeverfjord, G., 1996. Ryggdeformitet hos laks., AKVAFORSK-rapport. pp. pp18.

Aunsmo, A., Guttvik, A., Midtlyng, P.J., Larssen, R.B., Evensen, O., Skjerve, E., 2008. Association of spinal deformity and vaccine-induced abdominal lesions in harvest-sized Atlantic salmon, *Salmo salar* L. J. Fish Dis. 31, 515–524. https://doi.org/10.1111/j.1365-2761.2007.00899.x.

Baeverfjord, G., Åsgård, T., Rye, M., Storset, A., 1998a. High temperatures during egg incubation may induce malformations in Atlantic salmon (*Salmo salar* L.). in: Aquaculture and water. Abstract at Aquaculture Europe 98. EAS special publication no. 26. European Aquaculture Society, Oostende, Belgium., pp. 24-25.

Baeverfjord, G., Åsgård, T., Shearer, K.D., 1998b. Development and detection of phosphorus deficiency in Atlantic salmon, *Salmo salar* L., parr and post-smolts. Aquac. Nutr. 4, 1–11. https://doi.org/10.1046/j.1365-2095.1998.00095.x.

Baeverfjord, G., Åsgård, T., Shearer, K.D., 2009. Control of malformations in fish aquaculture: Science and practice. Fine Fish Project. www.feap.info/wp-content/uploads/2018/06/finefish.pdf (Access date: 15.11.2019).

Berg, A., Rødseth, O.M., Tangeras, A., Hansen, T., 2006. Time of vaccination influences development of adhesions, growth and spinal deformities in Atlantic salmon *Salmo salar*. Dis. Aquat. Org. 69, 239–248. https://doi.org/10.3354/dao069239.

Berg, A., Yurtseva, A., Hansen, T., Lajus, D., Fjelldal, P.G., 2012. Vaccinated farmed Atlantic salmon are susceptible to spinal and skull deformities. J. Appl. Ichthyol. 28, 446–452. https://doi.org/10.1111/j.1439-0426.2012.01988.x.

Bird, N.C., Mabee, P.M., 2003. Developmental morphology of the axial skeleton of the zebrafish, *Danio rerio* (Ostariophysi: Cyprinidae). Dev. Dyn. 228, 337–357. https://doi.org/10.1002/dvdy.10387.

Boglione, C., Gisbert, E., Gavaia, P.E., Witten, P., Moren, M., Fontagné, S., Koumoundouros, G., 2013. Skeletal anomalies in reared European fish larvae and juveniles. Part 2: main typologies, occurrences and causative factors. Rev. Aquac. 5, S121–S167. https://doi.org/10.1111/raq.12016.

Bou, M., Berge, G.M., Baeverfjord, G., Sigholt, T., Østbye, T.-K., Ruyter, B., 2017. Low levels of very-long-chain n-3 PUFA in Atlantic salmon (*Salmo salar*) diet reduce fish robustness under challenging conditions in sea cages. J. Nutr. Sci. 6, e32. https://doi.org/10.1017/jns.2017.28.

Bruno, D.W., 1990. Jaw deformity associated with farmed Atlantic salmon (*Salmo salar*). Vet. Rec. 126, 402–403.

Fjelldal, P.G., Hansen, T., Breck, O., Sandvik, R., Waagbø, R., Berg, A., Ørnsrud, R., 2009a. Supplementation of dietary minerals during the early seawater phase increase vertebral strength and reduce the prevalence of vertebral deformities in fast-growing under-yearling Atlantic salmon (*Salmo salar* L.) smolt. Aquac. Nutr. 15, 366–378. https://doi.org/10.1111/j.1365-2095.2008.00601.x.

Fjelldal, P.G., van der Meeren, T., Jørstad, K.E., Hansen, T.J., 2009b. A radiological study on vertebral deformities in cultured and wild Atlantic cod (*Gadus morhua*, L.). Aquaculture 289, 6–12. https://doi.org/10.1016/j.aquaculture.2008.12.025.

Fjelldal, P.G., Nordgarden, U., Wargelius, A., Taranger, G.L., Waagbø, R., Olsen, R.E., 2010. Effects of vegetable feed ingredients on bone health in Atlantic salmon. J. Appl. Ichthyol. 26, 327–333. https://doi.org/10.1111/j.1439-0426.2010.01430.x.

Fjelldal, P.G., Hansen, T., Breck, O., Ørnsrud, R., Lock, E.J., Waagbø, R., Wargelius, A., Eckhard Witten, P., 2012. Vertebral deformities in farmed Atlantic salmon (*Salmo salar* L.) – etiology and pathology. J. Appl. Ichthyol. 28, 433–440. https://doi.org/10.1111/j.1439-0426.2012.01980.x.

Gjerde, B., Pante, M.J.R., Baeverfjord, G., 2005. Genetic variation for a vertebral deformity in Atlantic salmon (*Salmo salar*). Aquaculture 244, 77–87. https://doi.org/10.1016/j.aquaculture.2004.12.002.

Grini, A., Hansen, T., Berg, A., Wargelius, A., Fjelldal, P.G., 2011. The effect of water temperature on vertebral deformities and vaccine-induced abdominal lesions in Atlantic salmon, *Salmo salar* L. J. Fish Dis. 34, 531–546. https://doi.org/10.1111/j.1365-2761.2011.01265.x.

Helland, S., Denstadli, V., Witten, P.E., Hjelde, K., Storebakken, T., Skrede, A., Åsgård, T., Baeverfjord, G., 2006. Hyper dense vertebrae and mineral content in Atlantic salmon (*Salmo salar* L.) fed diets with graded levels of phytic acid. Aquaculture 261, 603–614. https://doi.org/10.1016/j.aquaculture.2006.08.027.

Huntingford, F.A., Adams, C., Braithwaite, V.A., Kadri, S., Pottinger, T.G., Sandøe, P., Turnbull, J.F., 2006. Current issues in fish welfare. J. Fish Biol. 68, 332–372. https://doi.org/10.1111/j.0022-1112.2006.001046.x.

Kause, A., Ritola, O., Paananen, T., 2007. Changes in the expression of genetic characteristics across cohorts in skeletal deformations of farmed salmonids. Genet. Sel. Evol. 39, 529–543. https://doi.org/10.1051/gse:2007019.

Klebanoff, S.J., Kettle, A.J., Rosen, H., Winterbourn, C.C., Nauseef, W.M., 2013. Myeloperoxidase: a front-line defender against phagocytosed microorganisms. J. Leukoc. Biol. 93, 185–198. https://doi.org/10.1189/jlb.0712349.

Kvellestad, A., Hoie, S., Thorud, K., Torud, B., Lyngoy, A., 2000. Platyspondyly and shortness of vertebral column in farmed Atlantic salmon *Salmo salar* in Norway–description and interpretation of pathologic changes. Dis. Aquat. Org. 39, 97–108. https://doi.org/10.3354/dao039097.

Leven, D., Cho, S.K., 2016. Pseudarthrosis of the cervical spine: risk factors, Diagnosis and Management. Asian Spine J. 10, 776–786. https://doi.org/10.4184/asj.2016.10.4.776.

Lotz, J.C., Fields, A.J., Liebenberg, E.C., 2013. The role of the vertebral end plate in low back pain. Global Spine J. 3, 153–164. https://doi.org/10.1055/s-0033-1347298.

Madsen, L., Dalsgaard, I., 1999. Vertebral column deformities in farmed rainbow trout (*Oncorhynchus mykiss*). Aquaculture 171, 41–48. https://doi.org/10.1016/S0044-8486(98)00427-X.

Madsen, L., Arnbjerg, J., Dalsgaard, I., 2001. Radiological examination of the spinal column in farmed rainbow trout *Oncorhynchus mykiss* (Walbaum): experiments with Flavobacterium psychrophilum and oxytetracycline. Aquac. Res. 32, 235–241. https://doi.org/10.1046/j.1365-2109.2001.00552.x.

McKay, L.R., Gjerde, B., 1986. Genetic variation for a spinal deformity in Atlantic salmon, *Salmo salar*. Aquaculture 52, 263–272. https://doi.org/10.1016/0044-8486(86)90369-8.

Nordvik, K., Kryvi, H., Totland, G.K., Grotmol, S., 2005. The salmon vertebral body develops through mineralization of two preformed tissues that are encompassed by two layers of bone. J. Anat. 206, 103–114. https://doi.org/10.1111/j.1469-7580.2005.00372.x.

Quigley, D., 1997. A lower jaw deformity in juvenile and adult Atlantic Salmon (*Salmo salar* L.). Bull. Eur. Assoc. Fish Pathol. 15, 206–209.

Rentsch, C., Schneiders, W., Manthey, S., Rentsch, B., Rammelt, S., 2014. Comprehensive histological evaluation of bone implants. Biomatter 4, 10. https://doi.org/10.4161/biom.27993.

Roberts, R.J., Rodger, H.D., 2012. The pathophysiology and systematic pathology of Teleosts. In: Roberts, R.J. (Ed.), Fish Pathology. Blackwell Publishing Ltd. https://doi.org/10.1002/9781118222942.ch3.

Shaeib, F., Khan, S.N., Thakur, M., Kohan-Ghadr, H.R., Drewlo, S., Saed, G.M., Pennathur, S., Abu-Soud, H.M., 2016. The impact of myeloperoxidase and activated macrophages on metaphase II mouse oocyte quality. PLoS One 11, e0151160. https://doi.org/10.1371/journal.pone.0151160.

Silverstone, A.M., Hammell, L., 2002. Spinal deformities in farmed Atlantic salmon. Can. Vet. J. 43, 782–784.

Sullivan, M., Reid, S.W., Ternent, H., Manchester, N.J., Roberts, R.J., Stone, D.A., Hardy, R.W., 2007. The aetiology of spinal deformity in Atlantic salmon, *Salmo salar* L.: influence of different commercial diets on the incidence and severity of the preclinical condition in salmon parr under two contrasting husbandry regimes. J. Fish Dis. 30, 759–767. https://doi.org/10.1111/j.1365-2761.2007.00890.x.

Sutterlin, A.M., Holder, J., Benfey, T.J., 1987. Early survival rates and subsequent morphological abnormalities in landlocked, anadromous and hybrid (landlocked × anadromous) diploid and triploid Atlantic salmon. Aquaculture 64, 157–164. https://doi.org/10.1016/0044-8486(87)90351-6.

Takle, H., Baeverfjord, G., Lunde, M., Kolstad, K., Andersen, Ø., 2005. The effect of heat and cold exposure on HSP70 expression and development of deformities during embryogenesis of Atlantic salmon (*Salmo salar*). Aquaculture 249, 515–524. https://doi.org/10.1016/j.aquaculture.2005.04.043.

Toften, H., Jobling, M., 1996. Development of spinal deformities in Atlantic salmon and Arctic charr fed diets supplemented with oxytetracycline. J. Fish. Biol. 49, 668–677. https://doi.org/10.1111/j.1095-8649.1996.tb00063.x.

Trangerud, C., Bjørgen, H., Koppang, E.O., Grøntvedt, R.N., Skogmo, H.K., Ottesen, N., Kvellestad, A., 2020. Vertebral column deformity with curved cross-stitch vertebrae in Norwegian seawater-farmed Atlantic salmon, *Salmo salar* L. J. Fish. Dis. 43, 379–389. https://doi.org/10.1111/jfd.13136.

Vågsholm, I., Djupvik, H.O., 1998. Risk factors for spinal deformities in Atlantic salmon, *Salmo salar* L. J. Fish Dis. 21, 47–53. https://doi.org/10.1046/j.1365-2761.1998.00069.x.

Weisbrode, S.E., 2007. Pathology of organ systems, bone and joints. In: McGavin, M.D., Zachary, J.F. (Eds.), Pathological Basis of Veterinary Disease. Mosby Elsevier.

Witten, P.E., Gil-Martens, L., Hall, B.K., Huysseune, A., Obach, A., 2005. Compressed vertebrae in Atlantic salmon *Salmo salar*: evidence for metaplastic chondrogenesis as a skeletogenic response late in ontogeny. Dis. Aquat. Org. 64, 237–246. https://doi.org/10.3354/dao064237.

Witten, P.E., Gil-Martens, L., Huysseune, A., Takle, H., Hjelde, K., 2009. Towards a classification and an understanding of developmental relationships of vertebral body malformations in Atlantic salmon (*Salmo salar* L.). Aquaculture 295, 6–14. https://doi.org/10.1016/j.aquaculture.2009.06.037.

Witten, P.E., Fjelldal, P.G., Huysseune, A., McGurk, C., Obach, A., Owen, M.A.G., 2019. Bone without minerals and its secondary mineralization in Atlantic salmon (*Salmo salar*): the recovery from phosphorus deficiency. J. Exp. Biol. 222. https://doi.org/10.1242/jeb.188763.

Ytteborg, E., Baeverfjord, G., Torgersen, J., Hjelde, K., Takle, H., 2010a. Molecular pathology of vertebral deformities in hyperthermic Atlantic salmon (*Salmo salar*). BMC Physiol. 10, 12. https://doi.org/10.1186/1472-6793-10-12.

Ytteborg, E., Torgersen, J., Baeverfjord, G., Takle, H., 2010b. Morphological and molecular characterization of developing vertebral fusions using a teleost model. BMC Physiol. 10, 13. https://doi.org/10.1186/1472-6793-10-13.

Ytteborg, E., Torgersen, J.S., Pedersen, M.E., Helland, S.J., Grisdale-Helland, B., Takle, H., 2013. Exercise induced mechano-sensing and substance P mediated bone modeling in Atlantic salmon. Bone 53, 259–268. https://doi.org/10.1016/j.bone.2012.11.025.